CrystEngComm

Accepted Manuscript

ROYAL SOCIETY OF CHEMISTRY

www.rsc.org/crystengcomm

Journal Name

ARTICLE

Synthesis, color tunable emission, thermal stability, luminescence and energy transfer of Sm^{3+} and Eu^{3+} single-doped $M_3Tb(BO_3)_3$ (M = Sr and Ba) phosphors

Received 00th January 20xx,
Accepted 00th January 20xx

DOI: 10.1039/x0xx00000x

www.rsc.org/

Miaomiao Tian, Panlai Li*, Zhijun Wang*, Xiaoyun Teng, Zhenling Li, Jinge Cheng, Yuansheng Sun, Chao Wang, Zhiping Yang

A series of new tunable emission phosphors of Sm^{3+} and Eu^{3+} single-doped $M_3Tb(BO_3)_3$ (M = Sr and Ba) phosphors were synthesized by the solid-state reaction. Crystallization behavior and structure, reflectance spectral properties, luminescence properties, energy transfer, lifetimes, temperature dependent luminescence properties and CIE chromaticity coordinate of $M_3Tb(BO_3)_3:Ln^{3+}$ (M = Sr and Ba, Ln = Sm and Eu) were systematically investigated. $M_3Tb(BO_3)_3$ (M = Sr and Ba) crystallizes in a rhombohedral cell with space group R-3 by Rietveld structure refinement of the obtained phosphors with the standard data of $Ba_3Dy(BO3)_3$. $Sr_3Tb(BO_3)_3$ and $Ba_3Tb(BO_3)_3$ emit yellowish-green emission with the main peak around 555 nm and 550 nm, respectively, which originates from $^5D_4 \rightarrow {}^7F_4$ transition of Tb^{3+}, and $M_3Tb(BO_3)_3$: Ln^{3+}（Ln = Sm and Eu) phosphors show intense yellowish-green, yellow, orange and red emission with increasing Ln^{3+} concentration under 274 nm and 286nm excitation. The orange-red/red emissions peaked at 613nm ($Sr_3Tb(BO_3)_3:Sm^{3+}$, 627nm ($Sr_3Tb(BO_3)_3:Eu^{3+}$), 607nm ($Ba_3Tb(BO_3)_3:Sm^{3+}$) and 625nm ($Ba_3Tb(BO_3)_3:Eu^{3+}$) are contributed to the efficiently energy transfer Tb^{3+}-Sm^{3+} and Tb^{3+}-Eu^{3+}.The temperature dependent luminescence properties of $M_3Tb(BO_3)_3:Ln^{3+}$ have good thermal stabilities up to 150 °C, up to 72.8%. However, due to the defect in the host of $Sr_3Tb_{0.99}(BO_3)_3$:0.01Sm^{3+} phosphor, an amazing and interesting phenomenon can be observed that the emission intensity enhanced constantly with the increasing of temperature.

1. Introduction

Phosphor-converted white-light-emitting diodes (LEDs) are dominant candidates for replacing traditional light sources, due to the higher efficiency of energy conversion.[1-5] The color rending index (CRI) of commercial write LEDs using a blue LED chip and a yellow light-emitting phosphor are very poor, owing to the color insufficient in the red region.[6] An alternative approach involves the manufacture of ultraviolet (UV) LED chips by blending red-, green-, and blue-emitting phosphors to assemble white LEDs.[7] It is well known that the most effective excitation wavelength is 400 nm of InGaN LEDs.[8] However, LED emitting UV light ranging from 200 to 350 nm is commercially available despite of the poor external quantum efficiency. Thus it is significant to develop novel phosphors that can be excited efficiently under UV irradiation around 300 nm particularly red-emitting phosphors. So we focus on synthesizing $M_3Tb(BO_3)_3:Ln^{3+}$（Ln = Sm and Eu) under UV excitation from 220 to 350 nm, because it is found to be a novel efficiently orange-red emitting phosphor for UV-based LEDs. Rare earth borate matrix fluorescence powder is widely used which has many advantages, such as excellent product performance, low cost and easily made single doped double fluorescent powder. Consequently, in order to improve luminescence properties, the rare earth ions doping in borate was being widely studied and had broad prospects for development. Therefore, the Eu^{3+} and Sm^{3+} doped a single host lattice is a necessary research. Tb^{3+} performing as a yellowish-green emitter and at the same time as an efficient sensitizer to enhance the Sm^{3+} and Eu^{3+} red-emission would facilitate luminescence rendering and high quality color tunability light emission in co-doped with Sm^{3+} and Eu^{3+} of $M_3Tb(BO_3)_3$ (M = Sr and Ba). $M_3Tb(BO_3)_3$ (M = Sr and Ba) is an ideal host compound for this purpose, because the intense emission of $M_3Tb(BO_3)_3$ (M = Sr and Ba) of Tb^{3+} with a maximum at 555 nm meets well the above criterion. To fully understand the combined impacts of the doping concentration, and the energy transfer (ET) of Tb^{3+}-Sm^{3+} and Tb^{3+}-Eu^{3+} on luminescence of $M_3Tb(BO_3)_3:Ln^{3+}$ (M = Sr and Ba) were systematically investigated in the present work. Accordingly, tunable multicolor emission from yellowish-green to red in $M_3Tb(BO_3)_3:Ln^{3+}$ (M = Sr and Ba, Ln = Eu and Sm) phosphors can be realized upon UV excitation (274nm and 286nm) by using the allowed Tb^{3+} absorption transitions to sensitize Sm^{3+} and Eu^{3+} emission via ET of Tb^{3+} - Sm^{3+} and Tb^{3+} - Eu^{3+}. This investigation is a unique example of narrow line emitting phosphors under broad-band UV excitation allowing color tunability by controlled energy transfer.

[a] College of Physics Science & Technology, Hebei Key Lab of Optic-Electronic Information and Materials, Hebei University, Baoding 071002, China
+li_panlai@126.com; wangzj1998@126.com

† Footnotes relating to the title and/or authors should appear here.
Electronic Supplementary Information (ESI) available: [details of any supplementary information available should be included here]. See DOI: 10.1039/x0xx00000x

2. Experimental

2.1. Sample preparation

Samples of $M_3Tb(BO_3)_3$:Ln^{3+} (M = Sr and Ba) were prepared by the conventional high temperature solid state reaction. The starting materials $BaCO_3$ (99.9%), $SrCO_3$ (99.9%), Tb_4O_7 (99.99%)), H_3BO_3 (99.9%), Sm_2O_3 (99.99%) and Eu_2O_3 (99.99%) were mixed stoichiometrically with an excess of 5 mol % of H_3BO_3 as a flux. The above material stoichiometric ratio was measured by stoichiometric ratio, then it grinding for 20 minutes in the agate mortar, and evenly placed on a corundum crucible. The mixture was fired for 2 h at 850℃ in air. Remove the sample after cooling, after the uniform lapping in agate mortar, then reground and fired at 1200°C for 5 h with speed of 3°C per minute. It was cooled to room temperature and crushed to fine powder. The chemical reaction formula is as follows: [9]

$3MCO_3 + 3H_3BO_3 + 1/4Tb_4O_7 \rightarrow M_3Tb(BO_3)_3$ (M = Sr and Ba)

$3MCO_3 + 3H_3BO_3 + (1-x)/4Tb_4O_7 + x/2Sm_2O_3 \rightarrow M_3Tb_{1-x}(BO_3)_3$: xSm^{3+} (x = 0.001-0.1)

$3MCO_3 + 3H_3BO_3 + (1-y)/4Tb_4O_7 + y/2Eu_2O_3 \rightarrow M_3Tb_{1-y}(BO_3)_3$: yEu^{3+} (y = 0.001-0.1)

2.2. Materials Characterization

To analyze the phase structures of the as-prepared samples by the X-ray diffraction (XRD), which were carefully performed on D8-A25. Focus diffractometer (Bruker) measuring at 40KV and 40mA and recording the patterns in the range, 2θ = 10 ° to 80 °with scan rate of 0.05 °/s and step size of 0.01º. Measurements of excitation and emission spectra were recorded with a HITACHI F-4600 fluorescence spectrophotometer by a 450w Xe lamp as the excitation source, scanning at 240 nm/min and scanning wavelength from 200 to 700 nm. The temperature-dependent luminescence properties were measured on the same spectrophotometer which was assembled with a computer-controlled electric furnace and a self-made heating attachment. Luminescence decay curves of samples were measured by a Horiba FL-4600 fluorescence spectrophotometer using a LED as the excitation source. The diffuse reflection spectra were measured by a Hitachi U4100 UV-VIS-NIR Spectroscopy, with scanning wavelength from 200 to 700 nm. In addition, scanning electron micrograph (SEM) images were obtained using a Nova Nano SEM 650 LA and the fluorescent images of the paper were photographed with SLR camera of Canon in a dark environment.

3. Results and discussions

3.1. Crystallization behavior and structure

Figure 1 shows the representative XRD patterns of $M_3Tb(BO_3)_3$ (M= Sr, Ba), $Ba_3Lm(BO_3)_3$ (Lm = Tb, Dy) and $M_3Tb(BO_3)_3$ (M= Sr and Ba): Ln^{3+} (Ln = Sm and Eu). It is obvious that all the diffraction peaks of these samples can be testified to the pure structure with JCPDS card no. 50-0098, which indicates that the obtained samples are single phase and the introduced Sm^{3+}, Eu^{3+} can not cause any significant changes of host structure. The cell parameters of the $M_3Tb(BO_3)_3$ (M=Sr, Ba) and $Ba_3Lm(BO_3)_3$ (Lm = Tb, Dy) are listed in Table 1. However, there is a small shift to low diffraction degrees between $Ba_3Tb(BO_3)_3$ and $Ba_3Dy(BO_3)_3$, which is owing to the differences of ionic radius between Tb^{3+} and Dy^{3+} ($r_{Tb}^{3+} > r_{Dy}^{3+}$) in Figure 1a.[11-12] Based on the Prague equation : 2 d sinθ = n λ.[13] The ionic radii of Tb^{3+} (0.0923 Å, CN= 6) are similar to Dy^{3+} (0.0912Å, CN= 6).[14] Therefore, on the basis of charge and effective ionic radii of cations with different coordination numbers, it can be expected that the Tb^{3+} would occupy similar lattice sites to Dy^{3+} distributing in the host structure. Table 1 displays the plot of unit cell parameters versus the radius of the $Ba_3Tb(BO_3)_3$ (BTBO) and $Ba_3Dy(BO_3)_3$ (BDBO), the expected trend of decreasing unit-cell volume with decreasing ionic radius is observed, which indicates the "lanthanide contraction" takes effect. These results indicate that $Ba_3Tb(BO_3)_3$ and $Ba_3Dy(BO_3)_3$ have similar crystal structures and XRD patterns. Meanwhile, there is a small shift to high diffraction degrees between $Sr_3Tb(BO_3)_3$ (STBO) and $Ba_3Tb(BO_3)_3$ (BTBO), which is owing to the difference of ionic radius between Sr^{2+} and Ba^{2+} ($r_{Sr}^{2+} < r_{Ba}^{2+}$). With the Sr^{2+} constant substitution of Ba^{2+}, $Ba_3Tb(BO_3)_3$ gradually becomes $Sr_3Tb(BO_3)_3$.

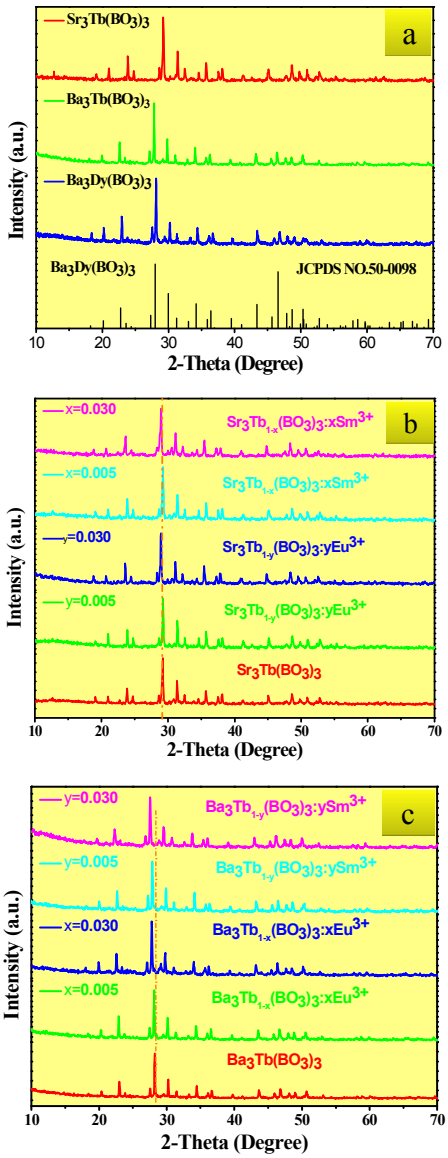

Figure 1 XRD patterns of $M_3Tb(BO_3)_3$ (M = Sr and Ba) and $Ba_3Dy(BO_3)_3$ with the standard data of $Ba_3Dy(BO_3)_3$ (JCPDS) No. 50-0098 (a), $Sr_3Tb(BO_3)_3$: Ln^{3+} (Ln = Sm and Eu) with the data of $Sr_3Tb(BO_3)_3$ (b), and $Ba_3Tb(BO_3)_3$: Ln^{3+} (Ln = Sm and Eu) with the data of $Ba_3Tb(BO_3)_3$ (c).

Table 1 Refinement Results of $M_3Tb(BO_3)_3$ (M=Sr,Ba) and $Ba_3Lm(BO_3)_3$ (Lm = Tb, Dy)

	$Sr_3Tb(BO_3)_3$	$Ba_3Tb(BO_3)_3$	$Ba_3Dy(BO_3)_3$
R_{wp}(%)	6.84	9.58	5.83
R_p(%)	5.18	6.86	4.10
X^2	3.812	3.365	1.510
Space group	R-3H	R-3H	R-3H
Lattice parameter (Å)			
a	12.522990	13.027461	13.041(3)
b	12.522990	13.027461	13.041(3)
c	9.253885	9.544923	9.523(2)
Cell params			
α	90°	90°	90°
β	90°	90°	90°
γ	120°	120°	120°
Cell Volume $(Å)^3$	1256.813	1402.887	1402.580
Z	6	6	6

The Sr-O distance is shorter than the Ba-O distance, leading to smaller lattice constants and stronger crystal field. According to Bragg's law,[13]

$$2d \sin\theta = n\lambda \quad (1)$$

where *d* is the distance between parallel lattice planes, ϑ is the diffraction angle (Bragg angle), *n* is the order of reflection (integer), and λ is the wavelength of X-rays. When Sr^{2+} was completely replaced by Ba^{2+}, the main peak appear right-shifted to a higher angle. It can be expected that the Sr^{2+} would occupy similar lattice sites Ba^{2+} distributing in the host structure in Figure 1a. These results indicate that $Sr_3Tb(BO_3)_3$, $Ba_3Tb(BO_3)_3$ and $Ba_3Dy(BO_3)_3$ have similar crystal structures and XRD patterns, and $Sr_3Tb(BO_3)_3$ and $Ba_3Tb(BO_3)_3$ have the similar type structure to $Ba_3Dy(BO_3)_3$ with no inversion symmetry.[10] Figure 1b and Figure 1c show the representative XRD patterns of $M_3Tb(BO_3)_3$:Ln^{3+} (M = Sr and Ba, Ln = Sm^{3+} and Eu^{3+}). It is obvious that all the diffraction peaks of these samples can be assigned to the pure structure with $M_3Tb(BO_3)_3$ (M = Sr, Ba), which indicates that the doped Sm^{3+} and Eu^{3+} can not cause any significant changes of host structure. However, there is a small shift to low diffraction degrees, which is due to the differences of ionic radius between Tb^{3+} and other rare earth ions ($r_{Sm}^{3+} > r_{Eu}^{3+} > r_{Tb}^{3+}$).[11,12] Based on equation (1), The ionic radii of Sm^{3+} (0.0958 Å, CN = 6) and Eu^{3+} (0.0947Å, CN = 6) are similar to Tb^{3+} (0.0923Å, CN = 6) respectively.[14] Therefore, on the basis of charge and effective ionic radii of cations with different coordination numbers, it can be expected that the doped Ln^{3+} would occupy similar lattice sites to Tb^{3+} distributing in the host structure. These results indicate that Ln^{3+} are undoubtedly doped into the $M_3Tb(BO_3)_3$ (M= Sr, Ba) crystal lattice.

The phase of as-prepared phosphor of $M_3Tb(BO_3)_3$ (M = Sr, Ba) were determined by Rietveld refinement.[15] The experimental and calculated diffraction XRD profiles for the $M_3Tb(BO_3)_3$ (M = Sr, Ba) are illustrated in Figure 2. The crystallo graphic data of $Ba_3Dy(BO_3)_3$ (ICSD-39740) is used as the model. $Ba_3Dy(BO_3)_3$ belongs to the R-3H symmetry and determines the same structure as $M_3Tb(BO_3)_3$ (M= Sr and Ba).[16-18] This calculated refinement using the Rietveld method evidences an excess of electron density due to the presence of heavier terbium on sites Sr1 (Ba1). However, Sr2 (Ba2) seems to be all- strontium (barium) , Tb2 seems to be all-terbium, oxygen atoms of the BO_3^{3-} anion in the structure are disordered over two positions with populations of 0.61 and 0.39, the boron atom takes a single position as shown in table 2.[19] It is observed that experimental data is uniformity with calculating data and the results are shown in Figure 2, Table 1 and Table 2. Consequently, the synthesized phosphors belong to trigonal system, and Space group is R-3H with Z= 6, and the refined unit cell parameters are a = 12.522990 Å, c = 9.253885 Å and V = 1256.813 $Å^3$ of $Sr_3Tb(BO_3)_3$ and a = 13.027461 Å, c = 9.544923 Å, and V = 1402.887 $Å^3$ of $Ba_3Tb(BO_3)_3$, which match well with those reported in the literature.[19] Therefore, structure parameters for $M_3Tb(BO_3)_3$ (M = Sr and Ba) as determined by Rietveld refinement of powder XRD data are identical with its real situation.

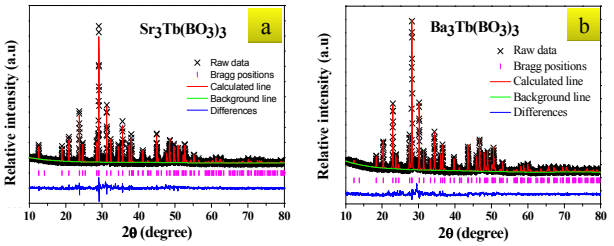

Figure 2 Rietveld analysis patterns for X-ray powder diffraction data of (a) $Sr_3Tb(BO_3)_3$ and (b) $Ba_3Tb(BO_3)_3$ compound. Solid red lines are calculated intensities, and crosses are the observed intensities. Short vertical lines show the position of Bragg reflections of the calculated pattern. Blue solid lines below the profiles stand for the difference between the observed and the

In order to further know the crystal structure and substitution of ions in $M_3Tb(BO_3)_3$ (M = Sr, Ba) host, Figure 3a shows the crystal structure of $Sr_3Tb(BO_3)_3$ and the coordination environment of cations (Tb2, Ba1/Tb1, and Ba2) and a schematic luminescence process from activator ions (A = Sm^{3+}/ Eu^{3+}) in a host crystal. The versatile $Sr_3Tb(BO_3)_3$ structure with its rigid open framework offers two types of sites for various cations to occupy, type one with trivalent Tb sites in TbO_6 polyhedra and type two with two different divalent Sr sites, and the coordination numbers of Sr1/Tb1, Sr2 and Tb2 atoms are 15, 12, 6 respectively. In this structure, the existence of different types of sites is proved to be available for the cations with different charge to occupy. It is found that the Sr1 (Tb1) atoms are coordinated forming Sr1 (Tb1) O15 groups with sharing edges on two O atoms with B atoms, and the B atoms are coordinated forming BO_6 groups, and they share edges or

Table 2 Refinement results, crystal structure data and SOF for $M_3Tb(BO_3)_3$ (M=Sr and Ba)

	Atom	Site	*x*	*y*	*z*	SOF
$Sr_3Tb(BO_3)_3$ (STBO)	Sr1/Tb1	18f	0.377232	0.259128	0.476901	0.8334/0.1666
	Tb2	3a	0.000000	0.000000	0.000000	1
	Sr2	3b	0.000000	0.000000	0.500000	1
	B1	18f	0.183606	0.179480	-0.142208	1
	O1	18f	0.122879	0.195924	-0.099190	0.61(2)
	O2	18f	0.268577	0.240435	-0.229906	0.61(2)
	O3	18f	0.065252	0.174754	-0.296541	0.61(2)
	O4	18f	0.035042	-0.009426	-0.083234	0.39(2)
	O5	18f	0.060749	0.198901	-0.353457	0.39(2)
	O6	18f	0.264681	0.250777	-0.312688	0.39(2)
$Ba_3Tb(BO_3)_3$ (BTBO)	Ba1/Tb1	18f	0.364972	0.243348	0.475302	0.8334/0.1666
	Tb2	3a	0.000000	0.000000	0.000000	1
	Ba2	3b	0.000000	0.000000	0.500000	1
	B1	18f	0.143725	0.185582	-0.355308	1
	O1	18f	0.058935	0.151424	-0.114298	0.61(2)
	O2	18f	0.234984	0.229132	-0.270591	0.61(2)
	O3	18f	0.023745	0.162812	-0.327985	0.61(2)
	O4	18f	0.147830	0.180855	-0.124129	0.39(2)
	O5	18f	0.130049	0.296155	-0.274508	0.39(2)
	O6	18f	0.358582	0.348971	-0.388491	0.39(2)

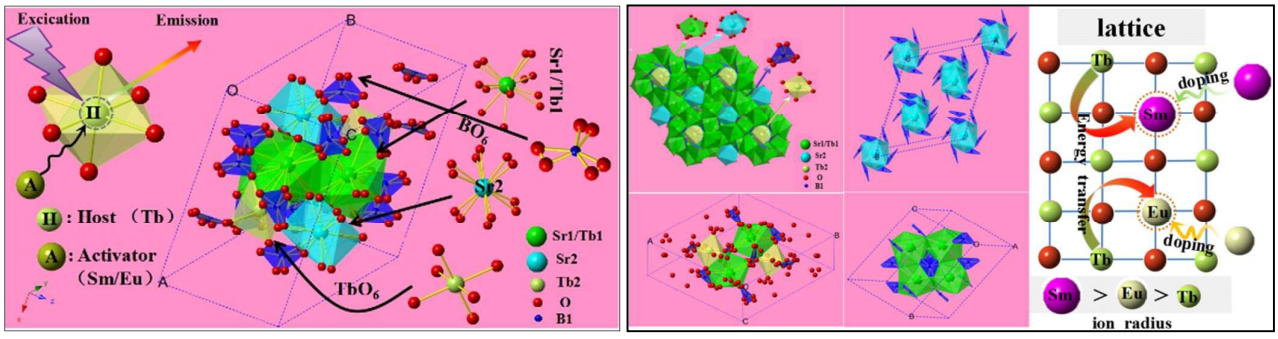

Figure 3 (a) Crystal structure of $Sr_3Tb(BO_3)_3$ emphasizing the coordination environment of cations (Tb1, Tb2, Ba1, B and Ba2); (b) the schematic explanation for the variation of the host lattice.

corners with Sr polyhedra to form a three-dimensional network as shown in Figure 3a and 3b. The borate group is regular with the average B-O distance 1.38(1) Å matching with the 1.378 Å deduced from crystal radii. The borate groups have the unique packing with the propeller pattern as seen in the Figure 3b. The most widely used activators are Sm^{3+} or Eu^{3+} ion, whose function in phosphors are to convert UV radiation to visible light as shown in Figure 3a. They also supply the possibility for doping RE ion, such as the coexistence of Tb^{3+}, Sm^{3+} and Tb^{3+}, Eu^{3+} in the open borate framework. In the present study, the ionic radii of Sr^{2+}, Tb^{3+}, Sm^{3+}, and Eu^{3+} are 1.49, 1.11, 1.25, and 1.15 Å, respectively. Therefore, it could offer the possible opportunity for Sm^{3+}-Tb^{3+} and Eu^{3+}-Tb^{3+} substitution due to the structure constraints when the $Sr_3Tb(BO_3)_3$:Sm^{3+} (Eu^{3+}) sample was prepared in the air. As shown in Table 2, Tb1 are distributed on individual Sr crystallographic sites, and some work on the explanation of the intrinsic mechanism is still in progress. A simple model to illustrate the spectra tuning mechanism of phosphors by controlling the doping level of Sm^{3+} or Eu^{3+} ion is shown in Figure 3b. Due to Sm^{3+} or Eu^{3+} ionic radii are bigger than that of host cation, the lattice expansion occur when doped Sm^{3+} or Eu^{3+} ion into the host lattice (Figure 3b).

The Scanning Electron Microscope (SEM) photographs morphology for the representative phosphors $Sr_3Tb(BO_3)_3$, $Ba_3Tb(BO_3)_3$, $Sr_3Tb_{0.99}(BO_3)_3$:1%Sm^{3+} and $Sr_3Tb_{0.98}(BO_3)_3$:2%Eu^{3+} are shown in Figure 4. The narrow size distribution and regular shape of the phosphor particles are important in application. It has been certified that optimum phosphor characteristics will be achieved with particle sizes on the order of 10-30 μm and spherical shape.[20] It is seen clearly that all of the samples are composed of aggregated grains with a uniform size distribution and an approximate sphere shape in these phosphors. Besides, the average particle size of our synthesized phosphors is about 30 μm, which meets the requirement well with the phosphors in application.

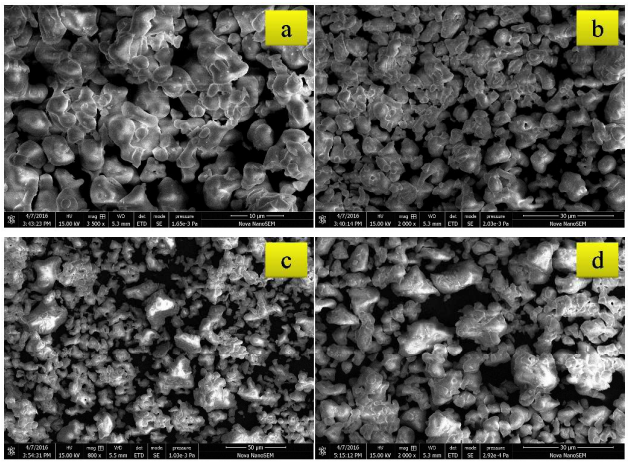

Figure 4 Typical SEM image of (a) $Sr_3Tb(BO_3)_3$, (b) $Ba_3Tb(BO_3)_3$, (c) $Sr_3Tb_{0.99}(BO_3)_3$:1% Sm^{3+} and (d) $Sr_3Tb_{0.98}(BO_3)_3$:2% Eu^{3+}.

3.2. Luminescence properties of $M_3Tb(BO_3)_3$ (M=Sr and Ba)

Figure 5 describes the emission and excitation spectra of $M_3Tb(BO_3)_3$ (M = Sr and Ba). First, we study the emission and excitation spectra of $Sr_3Tb(BO_3)_3$ in detail, as shown in Figure 5a and Figure 5b. The f-f electronic transitions cause the 286 nm excitation which displays a series of emission lines of Tb^{3+} ion with a main peak centered at 550 nm, which originates from the $^5D_4 \rightarrow {}^7F_5$ transition of Tb^{3+}.[21] And the emission spectrum with a weak broad band from the $^5D_3$ energy level is observed. The weak broad band ranging from 350 to 450 nm can be attributed to the occurrence of cross-relaxation with high concentration of Tb^{3+} ion. Monitored at 550 nm as shown in Figure 5b, the excitation spectrum of $Sr_3Tb(BO_3)_3$ exhibits one obvious broad band from 220 to 320 nm with the main peak at 286nm, and some weak band from 350 to 400 nm. The broad band with maxima at 286 nm should correspond to the spin-forbidden (high-spin, HS) $4f^8 - 4f^75d^1$ ($^7F_6 \rightarrow {}^9D$) transition with lower energy (ΔS = 1) of Tb^{3+} ion.[22,23] The other sharp lines in the long-wavelength regions can be assigned to the f–d transition of Tb^{3+} ion. And the remaining peaks are assigned to intra-$4f^8$ transitions between the $^7F_6$ and $^5D_{2,3,4}$ levels.[24] The above similar phenomenon has also been found in the $TbBO_3$ host.[22] The inset of Figure 5a is the image of $Sr_3Tb(BO_3)_3$ under 286 nm excitation, in which an intense yellowish-green light can be observed.

Figure 5c presents the emission and excitation spectra of $Ba_3Tb(BO_3)_3$. Monitored at 550 nm, the excitation spectrum of $Ba_3Tb(BO_3)_3$ displays a broad band (at 268nm) ranging from 220 to 320 nm, which is different from $Sr_3Tb(BO_3)_3$, and some weak peaks ranging from 350nm to 400nm. The broad band with maxima at 268 nm (f–d) should correspond to a spin-allowed (low-spin, LS) $4f^8 - 4f^75d^1$ ($^7F_6 \rightarrow {}^7D$) transition higher energy (ΔS = 0) of Tb^{3+} ion.[22-23] The sharp lines in the long-wavelength regions can be assigned to the f–f transition of Tb^{3+} ion. The emission spectrum presents the characteristic emission lines deriving from the 4f–4f transitions of Tb^{3+} ion in $Ba_3Tb(BO_3)_3$. The inset of Figure 3c depicts the obvious yellowish-green light of $Ba_3Tb(BO_3)_3$.

3.3. Reflectance spectra properties

The reflectance spectra of $M_3Tb(BO_3)_3$ (M = Sr and Ba), $Sr_3Tb_{0.99}(BO_3)_3$:0.01Sm^{3+}, $Sr_3Tb_{0.98}(BO_3)_3$:0.02Eu^{3+} are shown in Figure 6, which show the similar properties. The broad absorption bands of $M_3Tb(BO_3)_3$ (M=Sr and Ba) ranging from 200 to 300nm, due to the valence to conduction band transitions of the host in the UV region. Considering the same tendencies of $M_3Tb(BO_3)_3$:$y$$Eu^{3+}$, $M_3Tb(BO_3)_3$:$x$$Sm^{3+}$ (M = Sr and Ba) and $M_3Tb(BO_3)_3$, the host absorption band of $Sr_3Tb(BO_3)_3$:0.05Eu^{3+}, $Sr_3Tb(BO_3)_3$:0.05Sm^{3+} and $M_3Tb(BO_3)_3$ were calculated as the representative. The Kubelka-Munk absorption coefficient (K/S) relation is used to calculate the reflectance (R) for the host lattice:

$$K / S = (1-R)^2 / 2R \quad (2)$$

where K represents the absorption coefficient, S represents the scattering coefficient, and R represents the reflectivity. The inset of Figure 6 show the a plot of K/S for the $Ba_3Tb(BO_3)_3$,. $Sr_3Tb(BO_3)_3$ and $Sr_3Tb(BO_3)_3$:Ln^{3+} (Sm^{3+} and Eu^{3+}). The fundamental band gap energy (absorption edge) of $Sr_3Tb(BO_3)_3$ and $Ba_3Tb(BO_3)_3$ host are calculated to be approximately 5.82eV (213 nm) and 5.63ev (220 nm) by the K/S relation spectra, whilst the Sm^{3+} and Eu^{3+} doped $Sr_3Tb(BO_3)_3$ the band gap were are approximately 5.68ev (218 nm) and 5.54ev (224 nm). Obvious change of the band gap takes place between the ion-doped samples and the host. As a consequence, the ion-doped samples have the less band gap,

for the reason that the electron can more easily transfer from the valence band to the conduction band.

3.4. Luminescence properties of Sm^{3+}/Eu^{3+} in $M_3Tb(BO_3)_3$ (M = Sr and Ba).

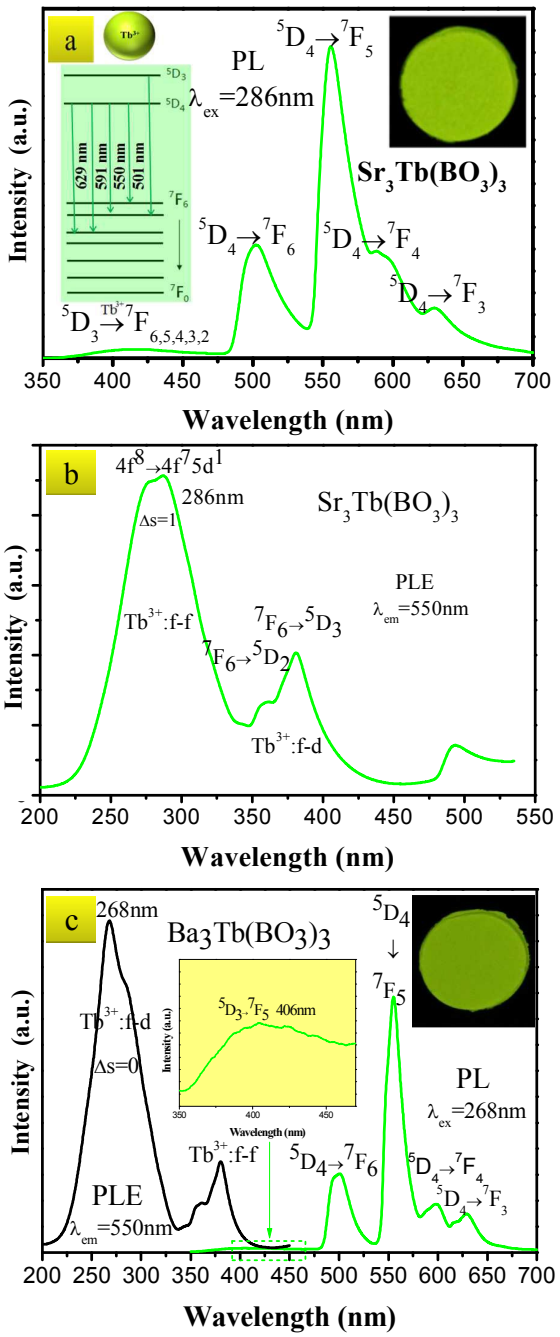

Figure 5 Emission spectra of $Sr_3Tb(BO_3)_3$（λ_{ex}=286 nm）(a), excitation spectra of $Sr_3Tb(BO_3)_3$ (λ_{em}=550 nm) (b) and emission and excitation spectra of $Ba_3Tb(BO_3)_3$（λ_{ex}=268nm, λ_{em}=550 nm）(c).

Figure 7(a) shows the excitation spectra of Sm^{3+} and Eu^{3+} ion singly doped phosphors, respectively, as well as the emission spectrum of $Sr_3Tb(BO_3)_3$. One can find that the spectral overlap between the emission spectrum of $Sr_3Tb(BO_3)_3$ and the excitation spectrum of $Sr_3Tb(BO_3)_3$:0.01Sm^{3+} and $Sr_3Tb(BO_3)_3$:0.02Eu^{3+} are observed, which indicate that the energy transfer from the Tb^{3+} to Sm^{3+} and Tb^{3+} to Eu^{3+} ion may be expected in Sm^{3+}/Eu^{3+} ion singly doped $Sr_3Tb(BO_3)_3$. According to Dexter's theory,[25] the effective resonant energy transfer is expected to take place from Tb^{3+} to Sm^{3+} and Tb^{3+} to Eu^{3+} ion. In order to indentify the existence of the energy transfer from Tb^{3+} to Sm^{3+} and Tb^{3+} to Eu^{3+}, the excitation spectrum of the Sm^{3+} and Eu^{3+} ion singly doped phosphors are monitored at 550, 613 and 627 nm, respectively. The excitation spectrum of Sm^{3+} is composed of seven bands peaking at 274, 287, 356，381，408，471 and 491 nm, respectively. The broad band at 274 nm is due to charge transfer state (CTS) of Sm^{3+}, and other sharp peaks are due to the 4f–4f inner shell transitions of Sm^{3+}. The excitation spectrum of Eu^{3+} consists of seven bands peaking at 274, 286, 358, 380, 471 and 495 nm, respectively. The broad band at 274 nm and other seven peaks are due to the CTS and the 4f–4f

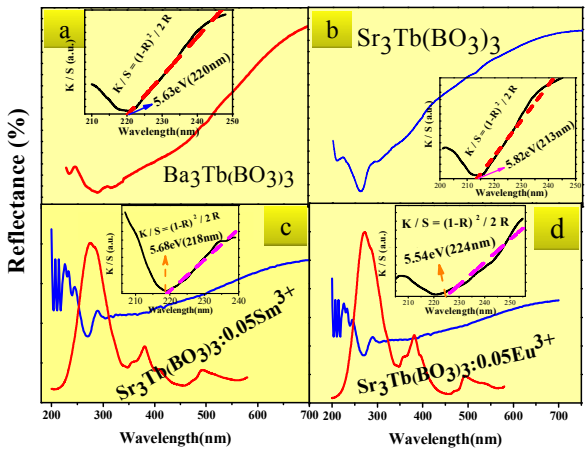

Figure 6 Diffuse reflection spectra of $M_3Tb(BO_3)_3$ (M=Sr and Ba), $Sr_3Tb_{0.99}(BO_3)_3$:0.01Sm^{3+} and $Sr_3Tb_{0.98}(BO_3)_3$:0.02Eu^{3+} samples. The inset show the a plot of K/S for the $Ba_3Tb(BO_3)_3$,. $Sr_3Tb(BO_3)_3$ and $Sr_3Tb(BO_3)_3$:Ln^{3+} (Sm^{3+} and Eu^{3+}).

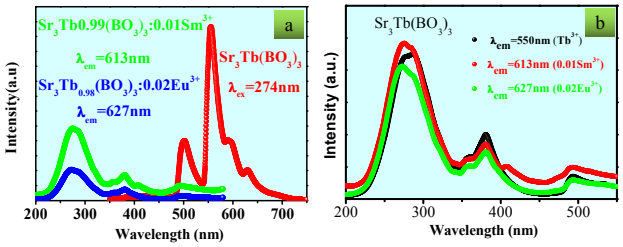

Figure7 (a) Emission spectra of $Sr_3Tb(BO_3)_3$ (λ_{ex} = 274 nm) and excitation spectra (λ_{em} = 613 nm) of $Sr_3Tb_{0.99}(BO_3)_3$:0.01Sm^{3+} and $Sr_3Tb_{0.98}(BO_3)_3$:0.02Eu^{3+} (λ_{em} = 627 nm), respectively. (b) Excitation spectra of $Sr_3Tb(BO_3)$ (λ_{em} = 550 nm), $Sr_3Tb(BO_3)$: Sm^{3+} (λ_{em} = 617 nm) and $Sr_3Tb(BO_3)$: Eu^{3+} (λ_{em} = 627 nm), respectively.

transitions of Eu^{3+}. The 356, 381 and 471 nm bands are associated with the transitions from the ground level $^7F_6$ to $^5D_2$,

$^5D_3$ and $^5D_4$ levels, respectively. In order to further confirmed above conclusion, Figure 7 (b) shows the comparison of excitation spectrum at 550 nm of $Sr_3Tb(BO_3)_3$, 613 nm of $Sr_3Tb_{0.99}(BO_3)_3$:0.01Sm^{3+} and 627 nm of $Sr_3Tb_{0.98}(BO_3)_3$: 0.02Eu^{3+}, respectively. It can be assumed that the emission peaks in the excitation spectrum of $Sr_3Tb(BO_3)_3$, $Sr_3Tb_{0.99}(BO_3)_3$:0.01Sm^{3+} and $Sr_3Tb_{0.98}(BO_3)_3$:0.02 Eu^{3+} are almost completely overlapped. In conclusion, the excitation peak of Tb^{3+} is also observed in the excitation spectrum (detected by the Sm^{3+} and Eu^{3+} emission), which demonstrates the phenomenon of energy transfer from Tb^{3+} to Sm^{3+} and Tb^{3+} to Eu^{3+} can occur.

For Ba_3Tb $(BO_3)_3$:Ln^{3+} (Ln = Sm^{3+} and Eu^{3+}) phosphors, there are the similar measurement data as $Sr_3Tb_{0.99}(BO_3)_3$:0.01Sm^{3+} and $Sr_3Tb_{0.98}(BO_3)_3$:0.02Eu^{3+}, as shown in Figure S1. The spectrum overlap between the emission spectrum of $Ba_3Tb(BO_3)_3$ and the excitation spectrum of $Ba_3Tb_{0.99}(BO_3)_3$:0.01Sm^{3+} and $Ba_3Tb_{0.98}(BO_3)_3$:0.02Eu^{3+} is observed, so we guess in the Ba_3Tb $(BO_3)_3$: Ln^{3+} (Ln = Sm^{3+} and Eu^{3+}), there may be energy transfer from Tb^{3+} to Sm^{3+} and Tb^{3+} to Eu^{3+}.

3.5. Energy transfer of $M_3Tb_{1-x}(BO_3)_3$: xSm^{3+} (M = Sr and Ba)

In order to further explain the energy transfer of $M_3Tb(BO_3)_3$:xSm^{3+} phosphors, the singly doped Sm^{3+} ion with different relative concentrations into the $Sr_3Tb(BO_3)_3$ was prepared. The emission spectra of the Sm^{3+} ion singly doped $Sr_3Tb(BO_3)_3$ samples under the excitation of 274nm are shown in Figure 8(a), which show a yellowish-green emission of Tb^{3+} ion and a red emission of Sm^{3+} ion in the emission spectra of $Sr_3Tb(BO_3)_3$:Sm^{3+}. The reddish orange light of Sm^{3+} (Figure 8a) is composed of 613 and 657 nm emission bands, corresponding to the $^4G_{5/2} \rightarrow {}^6H_J$ (J= 7/2 and 5/2) transitions, respectively. The emission intensity at 613 nm is the highest than that of other emission peaks of Sm^{3+} ion. The inset of Figure 8(a) shows the varying tendency of intensity of Tb^{3+} and Sm^{3+} in $Sr_3Tb_{0.99}(BO_3)_3$:xSm^{3+} depending on Sm^{3+} concentration. The intensity of Sm^{3+} gradually increased while the intensity of Tb^{3+} reduced with the increasing Sm^{3+} concentration, because the energy transfer from Tb^{3+} to Sm^{3+} take place. However, it can be observed that the emission intensity of the Sm^{3+} ion first increases to a maximum at x = 0.01, then decreases sharply with enhanced doping content, which is due to the concentration quenching effect. In general, the concentration quenching is the energy migration among the activator ion at the high concentration in Figure 8(c). With the continuous doping of Sm^{3+}, there is energy transduction from Sm^{3+} to Sm^{3+}, except for energy transfer Tb^{3+} - Sm^{3+}. Then Sm^{3+} ions have the same activated state in the host, and these energy states are closed enough and the energy transfer between states and quenching centers can occur with increasing of Sm^{3+} concentration. The energy becomes vibrational energy of the lattice which leads to the decrease of the luminous intensity.

There are the same phenomena of $Sr_3Tb_{1-x}(BO_3)_3$:Sm^{3+} in Ba_3Tb $(BO_3)_3$:Sm^{3+}, as shown in Figure S2a. The intensity of Tb^{3+} reduced and that of the Sm^{3+} ion first increases with increasing doping concentration, reaches a maximum at x = 0.01, then decreases sharply with the increasing Sm^{3+} concentration. The phenomenon of concentration quenching was also appeared. Therefore, there is energy transfer from Tb^{3+} to Sm^{3+} in the Ba_3Tb $(BO_3)_3$:Sm^{3+}.

3.6. Energy transfer mechanism of $M_3Tb_{1-y}(BO_3)_3$: yEu^{3+} (M=Sr and Ba)

We synthesized singly doped Eu^{3+} ion with different relative concentrations into the $M_3Tb(BO_3)_3$ host lattice, which used to prove energy transfer from Tb^{3+} to Eu^{3+}. Figure 8(b) exhibits the emission spectrum of the $Sr_3Tb(BO_3)_3$: yEu^{3+}. It shows yellowish-green emission band of Tb^{3+} ion and a red emission band of Eu^{3+} ion at the irradiation of 274 nm. The red emission peaks of Eu^{3+} ion are composed of 599, 627, and 712 nm, which belong to the $^5D_0 \rightarrow {}^7F_J$ (J=2, 3, 4) transitions, respectively, and the main emission is the 627 nm red peak.

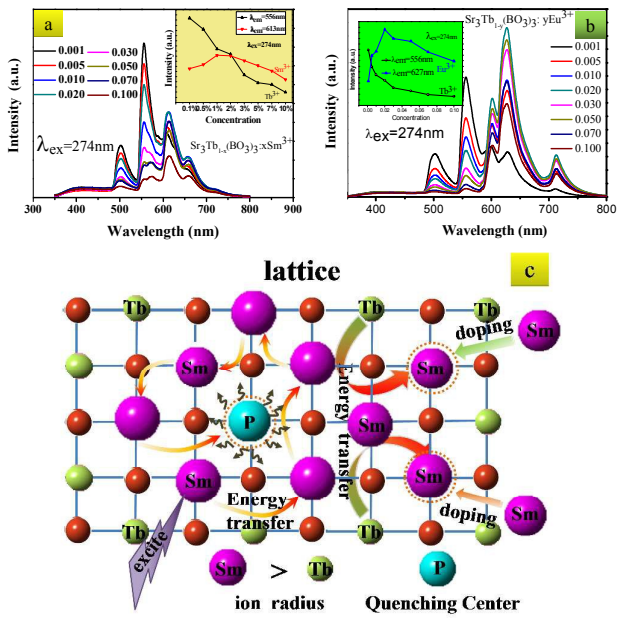

Figure 8 Emission spectra of Sm^{3+} (λ_{ex} = 274 nm) (a) and Eu^{3+} (λ_{ex} = 274 nm) (b), and the schematic diagram of concentration quenching process (c).

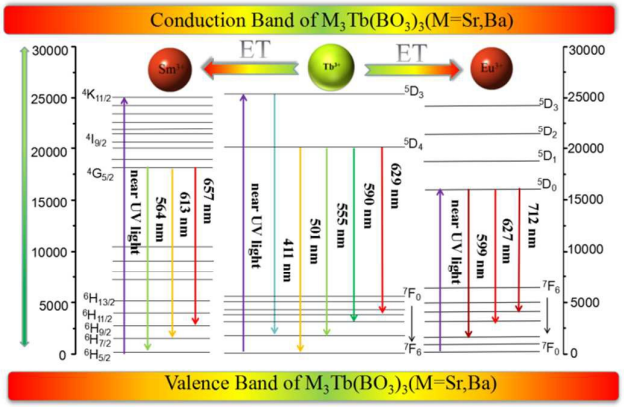

Figure 9 Schematic energy level diagram showing the energy transfer among Tb^{3+} to Sm^{3+} and Tb^{3+} to Eu^{3+} in $M_3Tb(BO_3)_3$:Ln^{3+} (M=Sr and Ba, Ln=Sm and Eu) phosphors.

It can be seen that the emission intensities at 556 nm of these series of phosphors decrease rapidly with increasing content of Eu^{3+} from 0.001 to 0.100 mol and the emission intensities at 627 nm of these series of phosphors increased rapidly with

increasing content of Eu^{3+} from 0.005 to 0.02 mol, and then declined dramatically with further increasing Eu^{3+} content, which indicates energy transfer from Tb^{3+} to Eu^{3+}, as shown in the inset of Figure 8(b). It is believed that the concentration quenching of Eu^{3+} and efficient Tb^{3+}- Eu^{3+} energy transfer can be used to explain the above Eu^{3+} doping concentration-dependent luminescence behavior, as shown Figure 8(c). Moreover, the energy transfer process is shown in Figure 9. The phenomenon of emission spectrum in the $Ba_3Tb_{1-y}(BO_3)_3$:yEu^{3+} was similar to $Sr_3Tb_{1-y}(BO_3)_3$:yEu^{3+}, as shown in Figure S2b. Therefore, there is energy transfer from Tb^{3+} to Sm^{3+} in the Ba_3Tb $(BO_3)_3$:yEu^{3+}. At the same time, the phenomenon of concentration quenching was also appeared.

To support the analysis above, Figure 10a gives the fluorescence decay curves of Tb^{3+} and Sm^{3+} by monitoring different wavelengths of 556 nm and 613 nm in $Sr_3Tb_{1-x}(BO_3)_3$: xSm^{3+}(x = 0.001-0.100) phosphors. It is found that all of the decay curves show a second-order exponential decay, which can be fitted by the equation:[26-28]

$$I(t) = I_0+A_1e^{-t/\tau1}+A_2e^{-t/\tau2} \quad (3)$$

where *I(t)* is the luminous intensity at time τ; A_1 and A_2 are constants; t is time, and τ_1 and τ_2 are lifetimes for rapid and slow decays, respectively. The decay process of these samples is characterized by an average lifetime τ*, which can be calculated using equation 4 as follows

$$\tau^* = (A_1\tau_1^2+A_2\tau_2^2) / (A_1\tau_1+A_2\tau_2) \quad (4)$$

On the basis of equation (4), the luminescence lifetime of Tb^{3+} in $Sr_3Tb(BO_3)_3$:xSm^{3+} decrease gradually with increasing Sm^{3+} concentrations shown in Figure 10(a). Then, the luminescence lifetime of Sm^{3+} in $Sr_3Tb_{1-x}(BO_3)_3$:xSm^{3+} with increasing Sm^{3+} concentrations firstly increase, and reach the maximum of x = 0.01, and then decreased due to the concentration quenching effect shown in Figure 10(b), which strongly demonstrates an energy transfer from Tb^{3+} to Sm^{3+}.

Similarly, Figure 11 shows the fluorescence decay curves of Tb^{3+} and Eu^{3+} at 556 nm and 627 nm in $Sr_3Tb_{1-y}(BO_3)_3$:yEu^{3+}. The decreasing average decay time of Tb^{3+} with increasing content of Eu^{3+} ion in $Sr_3Tb_{1-y}(BO_3)_3$:yEu^{3+} indicate the strengthening energy transfer (ET) from Tb^{3+} to Eu^{3+}. However, the luminescence lifetime of Eu^{3+} in $Sr_3Tb_{1-x}(BO_3)_3$:xEu^{3+} firstly increase, reach maximum value of x=0.02, and then decreased due to the concentration quenching effect shown in Figure 11(b). This is consistent with the concentration quenching of Sm^{3+} and Eu^{3+} in emission spectrum, which strongly demonstrates an energy transfer from Tb^{3+} to Eu^{3+}.

Figure S3 and Figure S4 show the fluorescence decay curves of Tb^{3+} and Ln^{3+} (Sm^{3+} and Eu^{3+}) emissions by monitoring the wavelengths at 550 nm , 607 nm and 625 nm in $Ba_3Tb(BO_3)_3$:Ln^{3+} phosphors. The phenomenon of the fluorescence decay curves in $Ba_3Tb(BO_3)_3$:Ln^{3+} was similar to $Sr_3Tb(BO_3)_3$:Ln^{3+}, which further proves the energy transfer from Tb^{3+} to Sm^{3+} and Tb^{3+} to Eu^{3+}.

In general, energy transfer from the sensitizer to activator in phosphors may take place via multipolar interaction or exchange interaction at high concentration. In order to determine the energy transfer mechanism in $M_3Tb(BO_3)_3$ samples, here is a detailed introduction of the $Sr_3Tb(BO_3)_3$ samples. It is necessary to know the critical distance (R_c) between activator and sensitizer such as Sm^{3+} and Tb^{3+}. When the distance is small enough, the concentration quenching occurs and the energy migration is hindered. Therefore, the calculation of R_c has been pointed out by Blasse:[29-31]

$$R_c = 2[3V/4\pi X_cN]^{1/3} \quad (5)$$

where V corresponds to the volume of the unit cell, N is the number of host cations in the unit cell, and X_c is the critical concentration of dopant ions. For the $Sr_3Tb(BO_3)_3$ host, N = 6, V = 1256.813 $Å^3$, and X_c is 0.01 for Sm^{3+}. Accordingly, R_c was estimated to be about 34.2 Å. Moreover, when the value of Sm^{3+} takes 0.10, that is to say, X_c is 0.10 for Sm^{3+}, R_c was estimated to be about 15.88Å. The results obtained above indicate the little possibility of exchange interaction between Tb^{3+} to Sm^{3+} since the exchange interaction is predominant only for about 5 Å. Thus the energy transfer from Tb^{3+} to Sm^{3+} may take place via the multipolar interaction.

In the same way, in the $Ba_3Tb(BO_3)_3$: xSm^{3+}, N = 6, V = 1402.887$Å^3$, and X_c is 0.01 for Sm^{3+}. As a result, the R_c value of Sm^{3+} in $Ba_3Tb(BO_3)_3$ is approximately 35.48 Å, which indicates the energy transfer from Tb^{3+} to Sm^{3+} may take place via the multipolar interaction.

The multipolar interaction could be the major mechanism of the concentration quenching for $Sr_3Tb_{1-x}(BO_3)_3$:xSm^{3+}. Dexter's theory proposed the emission intensity per activator follows the equation: [32, 33]

$$(I/x) = K[1+\beta(x)^{\theta/3}]^{-1} \quad (6)$$

when x is the activator concentration, I/x is the emission intensity per activator concentration, k and β are constants for a given host in the same excitation condition; and ϑ = 6, 8 and 10 represent the dipole-dipole, dipole-quadrupole and quadrupole-quadrupole interactions, respectively.

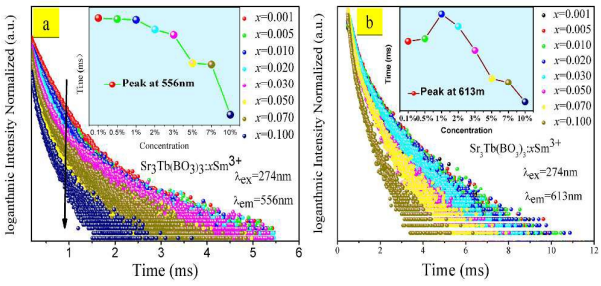

Figure 10 The luminescence lifetimes of Tb^{3+} (a) and Sm^{3+} (b) in $Sr_3Tb(BO_3)_3$:xSm^{3+}.

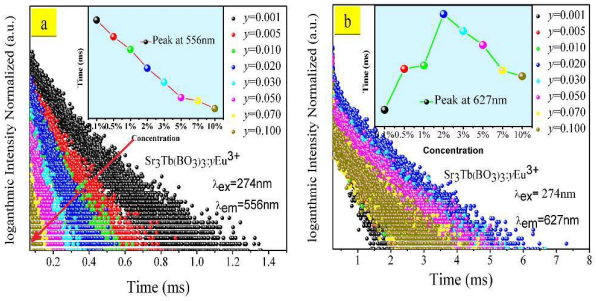

Figure 11 The luminescence lifetimes of Tb^{3+} (a) and Eu^{3+} (b) in $Sr_3Tb(BO_3)_3$:yEu^{3+}.

By modifying the Eq 6, log(I/x) acts a liner function of log(x) with a slop of (-θ/3). To get the value of θ, the relationship between log(I/x) and log(x) is plotted with x ranging from 0.01 to 0.10 in $Sr_3Tb_{1-x}(BO_3)_3$:xSm^{3+} and from 0.02 to 0.10 in Sr_3Tb_{1-}

$_y(BO_3)_3$:yEu^{3+}, respectively. Figure 12 shows the -ϑ/3 is -1.294 and -1.341 in $Sr_3Tb_{1-x}(BO_3)_3$:xSm^{3+} and $Sr_3Tb_{1-y}(BO_3)_3$:yEu^{3+}, Accordingly, θ is calculated to be 3.882 and 4.023 which are close to 6. The result indicates that the concentration quenching mechanism is the dipole – dipole interaction.[34-36]

The calculation by Dexter's theory as shown in Figure S5, relying on obtained results, it can be assumed that the -ϑ/3 is -1.3744 and -1.071 in $Ba_3Tb(BO_3)_3$:xSm^{3+} and $Ba_3Tb_{1-y}(BO_3)_3$:yEu^{3+}, Accordingly, θ is calculated to be 4.12 and 3.21 which are close to 6. The result indicates that the concentration quenching mechanism is the dipole-dipole interaction.

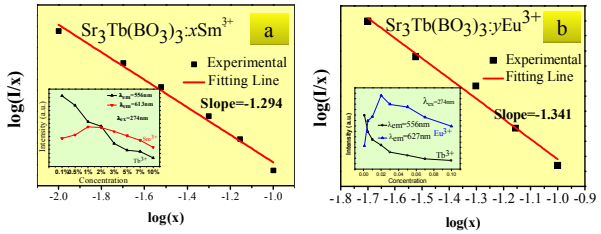

Figure 12 Plot of log (I/x) as function of log (x) in $Sr_3Tb(BO_3)_3$:xSm^{3+} and Sr_3Tb $(BO_3)_3$:yEu^{3+}. The inset is the emission intensities as function of Sm^{3+} (Eu^{3+}) concentration (λ_{ex} =274 nm).

3.7. Temperature dependence of luminescence properties

Thermal quenching is one of the important technological parameters for phosphors used in white LEDs.[37] It has considerable influence on the color rendering index and light output. The temperature dependence of emission spectra of $M_3Tb_{0.99}(BO_3)_3$:$0.01Sm^{3+}$ and $M_3Tb_{0.98}$ $(BO_3)_3$:$0.02Eu^{3+}$ (M = Sr and Ba) phosphors under 274 nm and 286 nm excitation were measured at temperature in the range of 20 – 300 °C, and the results are shown in Figure 13. The normalized emission intensities decrease with increasing temperature up to 300℃ of $M_3Tb_{0.98}(BO_3)_3$:$0.02Eu^{3+}$ and $Ba_3Tb_{0.99}(BO_3)_3$:$0.01Sm^{3+}$ phosphors. It can be clearly seen that the three phosphors have comparatively good temperature quenching effect, due to the emission intensity is found to be 94.3%, 72.8%, 85.2% of the initial value for $Sr_3Tb_{0.99}(BO_3)_3$:$0.01Sm^{3+}$ and $M_3Tb_{0.98}(BO_3)_3$:$0.02Eu^{3+}$(M = Sr and Ba), respectively, when the temperature increases up to 150℃. Generally speaking, the nonraditive transition probability by thermal activation is also strongly dependent on temperature, resulting in the decrease of emission intensity. However, the present $Sr_3Tb_{0.99}(BO_3)_3$:$0.01Sm^{3+}$ phosphor is not such a case. As given in Figure 14a, it represents the temperature dependence of the emission intensity gradually increase from room temperature to 150℃, and then increases slightly. The emission spectra variation of $Sr_3Tb_{0.99}(BO_3)_3$:$0.01Sm^{3+}$ from 20℃ to 300℃ is also given in Figure 13a, which not quench with the increasing temperature. This is an amazing and interesting phenomenon, and will be explained in detail below.

The half width at half maxima (FWHM) of $Sr_3Tb_{0.99}(BO_3)_3$:$0.01Sm^{3+}$ phosphors broaden gradually with increasing temperature in Figure 14b. It is well known that the thermally activated luminescent center strongly interact with the thermally active phonon, contributing to the variation of the FWHM of emission spectra.[38] At high temperature, the population density of phonon increases, and the interaction between electron and phonon is dominant, consequently the FWHM of emission spectrum is broadened. The insert of Figure 14b shows the mechanism configuration coordinate diagram of the FWHM of emission spectrum. Assuming that the ground state is v and the excited state is v', when the temperature increase, the system is in the higher vibrational state (v) of the ground state, and the transition can occur at a large scale, making the absorption spectra widened. In the corresponding emission process, electrons can relax on the higher vibration (v') in the excited state, which begin to transfer to the ground state, leading to the broadening of the emission spectrum. Therefore, the emission bandwidth depends on the ground state electron and phonon interaction. As the temperature increases, the phonon population density increases, and the interaction between the electron and the phonon strengthens, which brings about broadening of FWHM.

Figure 15 shows thermoluminescence (TL) glow curves monitoring Ln^{3+} (Ln = Sm and Eu) luminescence of the Ln^{3+}- doped $M_3Tb(BO_3)_3$ (M = Sr and Ba) and MTBO samples. Figure 15a shows the thermoluminescence glow curves of $Sr_3Tb(BO_3)_3$:xSm^{3+} (x = 0-0.1) in the range 150–300℃ and a TL band with the peak at 270℃ was observed when x=0. The TL peak originate from intrinsic defects in the $Sr_3Tb(BO_3)_3$ crystal. Obviously compared to the TL peak of the $Sr_3Tb(BO_3)_3$, the TL peaks of Sm^{3+} single doped STBO are shifted to lower temperature with changing Sm^{3+} content, and the TL peak from STBO: $0.01Sm^{3+}$ is 247℃. This result means that the trap depth of the electron trap center decreases with changing Sm^{3+} content.[39] Figure 15b are the thermoluminescence glow curves of

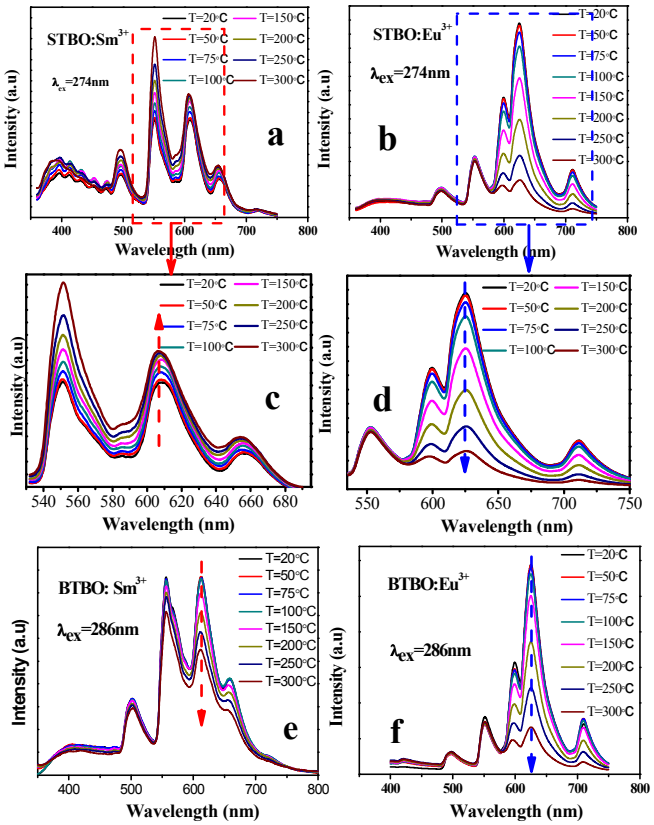

Figure 13 Temperature dependent luminescence properties of $Sr_3Tb_{0.99}(BO_3)_3$:$0.01Sm^{3+}$ (a), $Sr_3Tb_{0.98}(BO_3)_3$:$0.02Eu^{3+}$ (b), $Ba_3Tb_{0.99}(BO_3)_3$:$0.01Sm^{3+}$ (e) and $Sr_3Tb_{0.98}(BO_3)_3$:$0.02Eu^{3+}$ (f). (c) and (d) are the enlarged figure of (a) and (b), respectively.

$Sr_3Tb(BO_3)_3$:0.02Eu^{3+} and $Sr_3Tb(BO_3)_3$, which show the TL peak of $Sr_3Tb(BO_3)_3$:0.02Eu^{3+} at 302□, shifting to high temperature direction contrast with STBO. Figure 15c shows the TL curve of $Ba_3Tb(BO_3)_3$, $Ba_3Tb(BO_3)_3$:0.01Sm^{3+} and $Ba_3Tb(BO_3)_3$:0.02Eu^{3+} phosphors. It can be seen that these TL curves have three same peaks at 260□ and we do not observe the shift. The TL parameters of the thermal activation energy E which is associated with the trap depth can be derived from the equation of the thermoluminescence for a single trap depth, assuming no re-trapping, in the form: [40, 41]

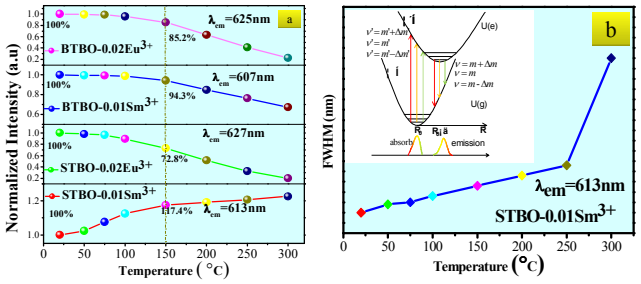

Figure 14 Temperature dependence tendency of normalized emission intensities of $M_3Tb_{0.99}(BO_3)_3$:0.01Sm^{3+} and $M_3Tb_{0.98}(BO_3)_3$:0.02Eu^{3+}(M=Sr and Ba) phosphors (a) and the FWHM of $Sr_3Tb_{0.99}(BO_3)_3$:0.01Sm^{3+} (b). The mechanism configuration coordinate diagram of the FWHM of emission spectrum in the inset of (b).

$$I(T) = S_{n0} \exp(-E_t / K_B T) \times [(l-1)s/\beta \times \int_{T0}^{T} \exp(-E_t/K_B T)dT+1]^{-l/(l-1)} \quad (7)$$

where *I(T)* is the TL intensity; *E* is the activation energy (trap depth); n_0 is the concentration of trap charges (electrons or holes) at t = 0; *s* is the frequency factor; k_B is the Boltzmann's constant; *b* is heating rate (1□/ s in this study), and *l* is the order of kinetics. In this paper, the effect of s on T_m (the temperature of curve peaking) is neglected and the frequency of an electron escaping from the trap is 1/s, the thermal activation energy E (eV) could be estimated by the formula of E = T_m(K)/500.[40] Hence the trap depth of $M_3Tb(BO_3)_3$, $M_3Tb(BO_3)_3$:0.01Sm^{3+} and $M_3Tb(BO_3)_3$:0.02Eu^{3+} (M = Sr and Ba) are 1.086eV ($Sr_3Tb(BO_3)_3$), 1.04eV ($Sr_3Tb(BO_3)_3$:0.01Sm^{3+}), 1.15eV ($Sr_3Tb(BO_3)_3$:0.01Eu^{3+}), 1.066eV ($Ba_3Tb(BO_3)_3$), 1.066eV ($Ba_3Tb(BO_3)_3$:0.01Sm^{3+}) and 1.066eV ($Ba_3Tb(BO_3)_3$:0.01Eu^{3+}), respectively, with the least value is 1.04 eV ($Sr_3Tb(BO_3)_3$:0.01Sm^{3+}). The $M_3Tb(BO_3)_3$ (M=Sr and Ba) is a native defect material which always has lattice defects such as the oxygen vacancy and the terbium–oxygen vacancy pair.[42,43] Figure 15d shows the schematic graph of energy band diagram of TL mechanism, and $Sr_3Tb(BO_3)_3$:0.01Sm^{3+} is the representative. The process represents the excitation state, when the sample absorbs energy (hv), electrons are excited to the conduction band with trapped by a trap (T), at the same time, the vacancies in the valence band are captured of luminescence center (L). Then the luminescence center is ionized and the electron trap is filled. The process of b is that electrons are released into the conduction band from the trap (T) under the thermal agitation. Then the electrons on the conduction band recombine the vacancies of the luminescent center (L) with thermoluminescence in the processes of c and e.

Here we analyze the phenomenon that the emission decreases in the PL emission spectra of $M_3Tb_{0.98}(BO_3)_3$:0.02Eu^{3+} and $Ba_3Tb_{0.99}(BO_3)_3$:0.01Sm^{3+} phosphors with the increasing temperature. The phenomenon can be ascribed to thermal quenching. It may be accounted for that deficiencies formed due to the radii mismatch between rare earth ions and cation ions.[44] As a result, the probability of non-radiative process increased, leading to the worse thermal stability. The temperature quenching mechanism could be explained by the configuration coordinate diagram shown in the Figure 16a. Because the slopes of the ground and the excited state are different, point F is the crossing point of the ground state

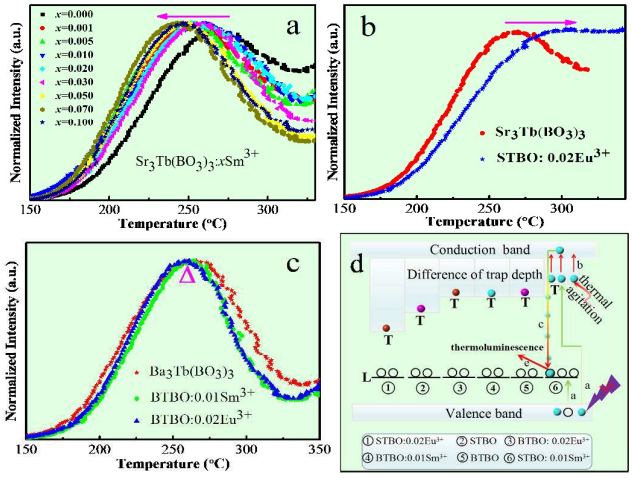

Figure 15 Thermoluminescence glow curves show Ln^{3+} (Ln = Sm and Eu) single doped MTBO and MTBO (M = Sr and Ba) and (d) the schematic graph of energy band diagram of TL mechanism.

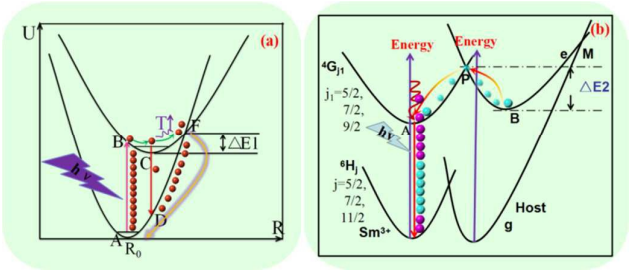

Figure 16 The configuration coordinate diagram of the temperature quenching of luminescence (a); the configurational coordinate diagram of the ground and excited states of Sm^{3+} and the defect in the $Sr_3Tb(BO_3)_3$ host (b).

and the excited state curves. With the increase of temperature, the phonon vibration will become more frequent and intense, and more electrons in an excited state absorb the phonon energy, and reach the intersection (F). Most electrons at state F can go back to the ground state (A) by non-radiative transition which is strongly favored in high temperature, resulting in the decrease of emission intensity.[40] However, its detailed luminescence mechanism and process are intriguing enough to further explore in the future.

Especially, the as-prepared $Sr_3Tb_{0.99}(BO_3)_3$:0.01Sm^{3+} phosphor has the abnormal temperature dependent emission property. Emission intensity of $Sr_3Tb_{0.99}(BO_3)_3$:0.01Sm^{3+} increases quickly from room temperature to 150 ℃, and then increases slightly. That is, there is no temperature quenching. The temperature quenching mechanism and the abnormal temperature dependent emission property could be explained by the configuration coordinate diagram shown in the Figure 16b. In order to simplify the discussion, only one crossing point of e and the excited states of Sm^{3+} (P) are marked. $^6H_{j1}$ (j_1 = 5/2,

7/2 and 9/2) represent the ground of Sm^{3+} and ^4G_j (j =11/2, 7/2 and 5/2) represent the excited states of Sm^{3+} in the curves, respectively. The curves g and e represent the ground and excited states of the lattice defects in the STBO host, respectively. Points A and B are the positions equilibrium lattice of ^4F_j and e curves, respectively. Point M is the crossing point of curves e and g, while point P is the crossing point of curves e and the excited states of Sm^{3+}. At room temperature, the electrons in ^6H_j and g are firstly excited to their excited states under 274 nm excitation, then most of the electrons return to their ground states via radiative transition in the excited states of Sm^{3+}. However, with the increase of the temperature, most electrons in excited state e are strongly favored to overcome the energy barrier ΔE2, in addition to the radiative transition, because the least value of the trap depth of $Sr_3Tb(BO_3)_3$:0.01Sm^{3+} is 1.04eV in $M_3Tb(BO_3)_3$:Ln^{3+} and the electrons are easily released into the conduction band from the trap (T) under the thermal agitation. Then the electrons on the conduction band recombine with the vacancies of the luminescent center (L) with luminescence. So most electrons in excited state e transfer their energy to ^6H_j due to electron–phonon coupling, thereby, the emission intensity of Sm^{3+} is enhanced. In summary, with an increase in temperature, more and more electrons in excited state e can overcome energy barrier ΔE2 due to stronger electron–phonon coupling, and transfer energy from the crossing point to the excited states of Sm^{3+} and Tb^{3+}, which slow down the decline of the emission intensity of Sm^{3+} and Tb^{3+}, consequently.

In order to understand the temperature dependence of emission intensity and to determine the activation energy for thermal quenching, the Arrhenius equation was fitted to the thermal quenching data of $Ba_3Tb_{0.99}(BO_3)_3$:0.01Sm^{3+} and $M_3Tb_{0.98}(BO_3)_3$:0.02Eu^{3+} (M=Sr, Ba) phosphors, as shown in Figure 17.[45-46] As demonstrated in eq 8, the probability of thermal activation is strongly dependent on temperature, resulting in the decrease of emission intensity.

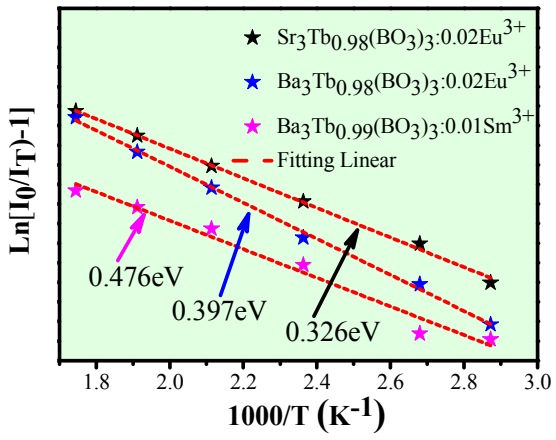

Figure 17 Activation energy for thermal quenching of $M_3Tb_{0.98}$ $(BO_3)_3$:0.02Eu^{3+} (M=Sr and Ba) and $Ba_3Tb_{0.99}(BO_3)_3$:0.01Sm^{3+} phosphors.

$$I_T = I_0/1+c\exp(-\Delta E/k\,T) \quad (8)$$

In eq 8, I_0 is the initial emission intensity, I_T is the intensity at different temperatures, ΔE is activation energy of thermal quenching, c is a constant for a certain host, and k is the Boltzmann constant (8.629×10^{-5} eV). Figure 17 plots the relationship of Ln $[(I_0/I_T)-1]$ versus 1000/T for the phosphors, which is linear with a slope of 3.789 ($Sr_3Tb_{0.98(}BO_3)_3$:0.02Eu^{3+}), 4.609 ($Ba_3Tb_{0.98(}BO_3)_3$:0.02Eu^{3+}) and 5.523 ($Ba_3Tb_{0.98(}BO_3)_3$:0.02Sm^{3+}). According to eq 8, the activation energy ΔE1 was calculated to be 0.327 eV, 0.397 eV and 0.4766 eV. Usually, ΔE1 is related to the energy gap between the lowest energy Eu^{3+} and Sm^{3+} excited level and the bottom of the conduction band, which is connected with thermally activated energy transfer processes. Thus, $M_3Tb_{0.98(}BO_3)_3$:0.02Eu^{3+} and $Ba_3Tb_{0.98(}BO_3)_3$:0.01Sm^{3+} phosphors have a high or comparable activation energy value, which show that this series of $M_3Tb_{0.99}(BO_3)_3$:0.01Sm^{3+} and $M_3Tb_{0.98}(BO_3)_3$:0.02Eu^{3+} phosphors have excellent thermal stability.

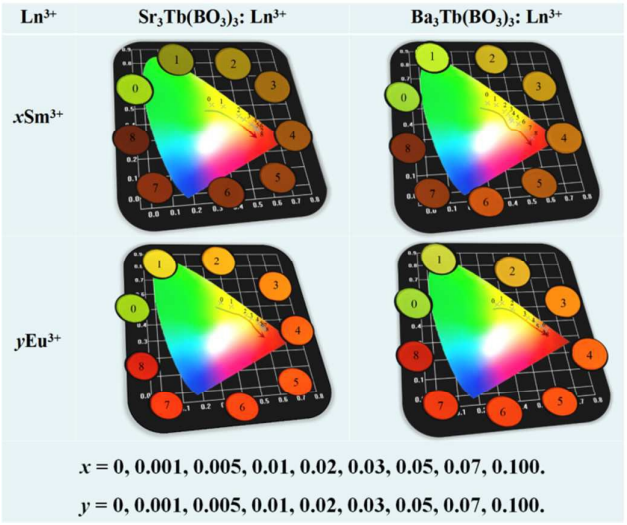

Figure 18 CIE chromaticity coordinate of $Sr_3Tb(BO_3)_3$:Ln^{3+} and $Ba_3Tb(BO_3)_3$:Ln^{3+} (Ln = Sm^{3+} and Eu^{3+}) (λ_{ex} = 254 nm).

3.8. CIE chromaticity coordinate

Energy transfer makes it possible to obtain both yellowish-green emission of Tb^{3+} ion and red emission of Sm^{3+} and Eu^{3+} ions in a single host, which is a feasible route to realize color-tunable emission under excitation of UV radiation. This result also confirmed by the CIE chromaticity coordinates shown in Figure 18. The photographs illustrate the color-tunability under 254 nm excitation with a UV lamp for $Sr_3Tb(BO_3)_3$:Ln^{3+}(Ln = Sm^{3+} and Eu^{3+}) and $Ba_3Tb(BO_3)_3$:Ln^{3+} (Ln = Sm^{3+} and Eu^{3+}) phosphors with different Ln^{3+}(Ln = Sm^{3+} and Eu^{3+}) content in Figure 18. Their emission color can tune from yellowish-green to red or orange-red, which is attributed to the efficient energy transfer from Tb^{3+} to Sm^{3+} and Eu^{3+}, respectively. And the variation of color can be clearly observed by the naked eye. The CIE coordinates vary systematically from yellowish-green to red or orange-red for $M_3Tb(BO_3)_3$:Ln^{3+} (M = Sr and Ba, Ln = Sm^{3+} and Eu^{3+}) with the variation of Ln^{3+} ions concentration. The results indicate that the phosphor may serve as potential red or orange-red emitting materials for UV based white LEDs.

Conclusions

The new tunable emission phosphors of $M_3Tb(BO_3)_3$:Ln^{3+}（M = Sr and Ba，Ln = Sm and Eu) were synthesized by the conventional solid-state reaction, and the Rietveld method were successful refined the crystal structures for $M_3Tb(BO_3)_3$:Ln^{3+} (M = Sr and Ba，

Ln = Sm and Eu). The color can be varied from yellowish-green to red or orange-red depending on the relative content of Ln^{3+} in the host. Under 274 nm and 286 nm UV light excitation, $M_3Tb(BO_3)_3:Ln^{3+}$ (M = Sr and Ba) phosphors exhibit greenish-yellow and red light with peaks at 501, 555, 613, 657 and 725 nm for $Sr_3Tb(BO_3)_3:Sm^{3+}$ and $Ba_3Tb(BO_3)_3:Sm^{3+}$. And under 274 nm and 286 nm UV light excitation, $M_3Tb(BO_3)_3:Eu^{3+}$ (M = Sr and Ba) phosphors exhibit greenish-yellow and red light with peaks at 501, 555, 599, 603, 627 and 713 nm for $Sr_3Tb(BO_3)_3:Eu^{3+}$ and $Ba_3Tb(BO_3)_3:Eu^{3+}$. The interesting luminescence behavior should be ascribed to efficient energy transfer of Tb^{3+}- Sm^{3+} and Tb^{3+}- Eu^{3+} in $M_3Tb(BO_3)_3:Ln^{3+}$ phosphors. In addition, the luminescence properties of $M_3Tb(BO_3)_3:Ln^{3+}$ have high thermal quenching temperatures. The results indicate that the novel borate phosphors may serve as potential red or orange-red emitting material for UV based white LEDs.

Acknowledgements

The work is supported by the National Natural Science Foundation of China (No.50902042), the Funds for Distinguished Young Scientists of Hebei Province, China (No.A2015201129), the Natural Science Foundation of Hebei Province, China (Nos.A2014201035, E2014201037), the Education Office Research Foundation of Hebei Province, China (Nos.ZD2014036, QN2014085), China Postdoctoral Science Foundation funded project (No.2015M581311), the Midwest Universities Comprehensive Strength Promotion Project.

Notes and references

1 C. C.Lin, R.-S.Liu and J. Phys. Chem. Lett. 2011, 2, 1268 −1277.
2 T. Hashimoto, F. Wu, J. S. Speck and S. Nakamura, Nat. Mater. 2007, 6, 568 −571.
3 H. A. Höppe and Angew. Chem., Int. Ed. 2009, 48, 3572 −3582.
4 S. Ye, F. Xiao, Y. X. Pan, Y. Y. Ma and Q. Y. Zhang, Mater. Sci. Eng. R 2010, 71,1 −34.
5 W.-Y. Huang, F. Yoshimura, K. Ueda, Y. Shimomura, H.-S. Sheu, T.-S. Chan, C.-Y. Chiang, W. Zhou and R.-S. Liu, Chem. Mater. 2014, 26, 2075 −2085.
6 (a) G. Blasse and A. Bril, J. Chem. Phys. 1967, 47, 5139. (b) A. A. Setlur, W. J. Heward, Y. Gao, A. M. Srivastava, R. G. Chandran and M. V. Shankar, Chem. Mater. 2006, 18, 3314.
7 (a) M. P. Saradhi and U. V. Varadaraju, Chem. Mater. 2006, 18, 5267. (b) C. H. Huang, and T. M. Chen, Inorg. Chem. 2011, 50, 5725. (c) W. R. Liu, C. H. Huang, C. P. Wu, Y. C. Chiu, Y. T. Yeh and T. M. Chen, J. Mater. Chem. 2011, 21, 6869.
8 (a) D. S. Kang, H. S. Yoo, S. H. Jung, H. K. Kim and D. Y. Jeon, J. Phys. Chem. C 2011, 115, 24334. (b) F. P. Du, R. Zhu, Y. L. Huang, Y. Tao and H. J. Seo, Dalton Trans. 2011, 40, 11433.
9 D. Zhao, Z. Hu, Z. Lin and G. J. Wang, Cryst. Growth. 2005, 277, 401-405.
10 Y. N. Xue, F. Xiao and Q. Y. Zhang, Spectrochim. Acta. Part. A. 2011, 78, 1445-1448.
11 P. Boutinaud, L. Sarakha, R. Mahiou, P. Dorenbos and Y. Inaguma, J. Lumin. 2010, 130, 1725-1729.
12 G. F. Ju, Y. H. Hu, L. Chen, X. J. Wang and Z. F. Mu, Mater. Res. Bull. 2013, 48, 4743-4748.
13 J. Kacher, C. Landon, B. L.Adams and D. Fullwood, Ultramicroscopy, 2009, 109, 1148-1156.
14 R. D. Shannon, Acta Crystallogr. Sect. A: Cryst. Phys., Diffr., Theor. Gen. Crystallogr. 1976, 32, 751.
15 C. Larson and R. B. Von Dreele, Los Alamos National Laboratory Report LAUR, Los Alamos National Laboratory: Los Alamos, 2000, 86, 748-789.
16 A. Bessiere, R. A. Benhamou, G. Wallez, A. Lecointre and B. Viana, Acta Mater. 2012, 60, 6641-6649.
17 Z. H. Xu, C. X. Li, Z. Y. Hou, C. Peng and J. Lin, CrystEngComm. 2011,13, 474-482.
18 A. V. Teterskii, S. Yu. Stefanovich, B. I. Lazoryak and D. A. Rusakov, Russ. J. Inorg. Chem. , 2007, 52(3), 308–314.
19 Khamaganova T N, Khrushcheva N M, Astakhov, N. E. Russ. J. Appl. Chem. 2009, 82:2214-2216.
20 Y. C. Kang, S. B. Park, I. W. Lenggoro, and K. Okuyama, J. Phys. Chem. Solids, 1999, 60, 379–84.
21 (a) G. G. Li, D. L. Geng, M. M. Shang, Y. Zhang, C. Peng, Z. Y. Cheng and J. Lin, J. Phys. Chem. C 2011, 115, 21882. (b) H. Y. Chuang, C. H. Lu and C. H. Hsu, J. Am. Ceram. Soc. 2010, 93, 1838.
22 J .Yang, C. M. Zhang, C. X. Li and J. Lin, Inorg. Chem. 2008, 47,7262.
23 (a) C. H. Hsu and C. H. Lu, J. Mater. Chem. 2011, 21, 2932.(b) W. B. Park, S. P. Singh, M. Pyo and K. S. Sohn, J. Mater. Chem. 2011, 21, 5780.
24 Y. Jia, W. Lu, N. Guo, W. Lü, Q. Zhao and H. Yoü, Phys. Chem. Chem. Phys., 2013, 15, 6057–6062.
25 G. Blasse. J. Lumin., 1976, 14, 231-233.
26 X. Liu, C. Li, Z. Quan, Z. Cheng and J. Lin. J. Phys. Chem. C, 2007, 111, 16601-16607.
27 X. Liu, L. Yan and J. Lin. J. Phys. Chem. C, 2009, 113, 8478-8483.
28 M. Yu, J. Lin and J. Fang. Chem. Mater., 2005, 17, 1783-1791.
29 G. Blasse and B. Grabmaier. Luminescent materials, Springer,1994.
30 G. Blasse. Phys. Lett. A, 1968, 28, 444-445.
31 Z. G. Xia, Y. J. Liang, D. Y. Yu, M. F. Zhang, W. Z. Huang, M. H.Tong, J. M. Wu and J. W. Zhao. Opt. Laser Technol., 2014, 56, 387-392.
32 L.G. Van Uitert, J. Electrochem. Soc. 1967, 114, 1048–1053.
33 L. Ozawa and P.M. Jaffe, J. Electrochem. Soc. 1971, 118, 1678–1679.
34 J. Zhou and Z. G. Xia, J.mater.chem.c, 2015, 3, 7552-7560.
35 J. Zhou and Z. G. Xia, J.mater.chem.c, 2014, 2, 6978-6984.
36 Z. G. Xia, J. Q. Zhuang, and L. B. Liao, Inorg. Chem, 2012, 51, 7202-7209.
37 (a) D. Y. Wang, C. H. Huang, Y. C. Wu and T. M. Chen, J. Mater. Chem., 2011, 21, 10818; (b) J. Y. Han, W. B. Im, D. Kim, S. H. Cheong, G. Y. Lee and D. Y. Jeon, J. Mater. Chem., 2012, 22, 5374.
38 V. B. Mikhailikm, H. Kraus, D. Wahl, M. Itoh, M. Koike and I. K. Bailiff, Phys. Rev. B 2004, 69, 205110.
39 Xu J, Ueda J, Kuroishi and S.Tanabe, Appl. Phys. Lett. 2014, 04, 101904.
40 M.S. Jahan, D.W. Cooke, W.L. Hults, J.L. Smith, B.L. Benneth and M.A. Maez, J. Lumin. 1990, 47, 85–91 .
41 D.W. Cooke, B.L. Bennett, E.H. Farnum, W.L. Hults, R.E. Muenchausen and J.L. Smith, Appl. Phys. Lett. 1997,70, 3594–3596.
42 Y.Y. Lu, F. Liu, Z. Gu and Z. Pan, J. Lumin. 2011, 131, 2784–2787.
43 C.H. Liang, G.W. Meng, G.Z. Wang, Y.W. Wang, L.D. Zhang and S.Y. Zhang, Appl. Phys. Lett. 2001, 78, 3202–3204.

44 Y. Y. Li, Q. S. Wu, X. C. Wang, J. Y. Ding, Q. Long and Y. H. Wang, RSC Adv., 2014, 4, 63569-63575.
45 B. Henderson and G. F. Imbusch, Clarendon Press: Oxford, 1989.
46 Y. Chen, B. Liu, C. Shi, G. Ren, and G. Zimmerer, Nucl. Instrum. Methods Phys. Res. Sect. A 2005, 537, 31.

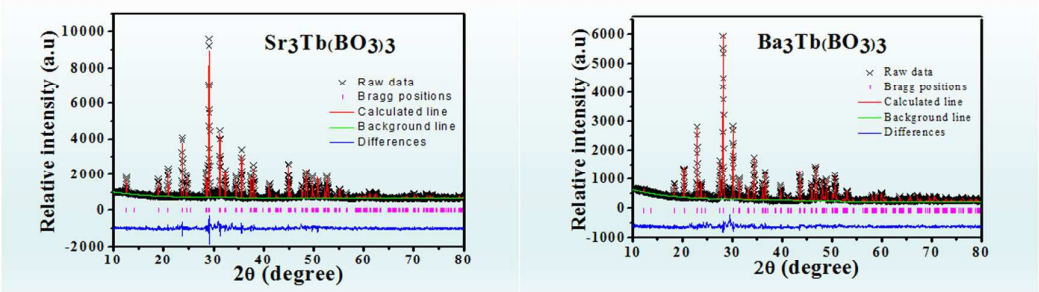

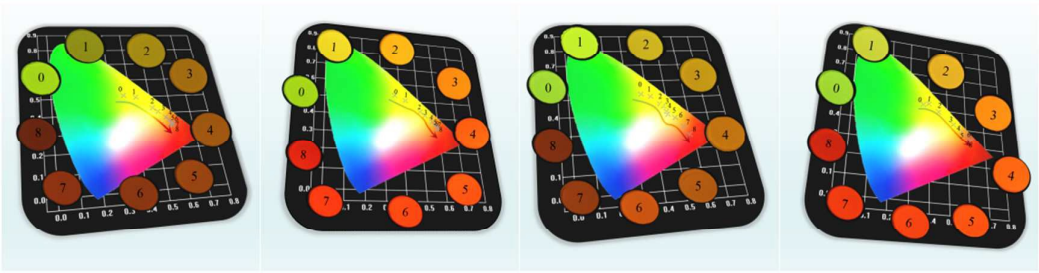

$Sr_3Tb(BO_3)_3$: xSm^{3+}	$Sr_3Tb(BO_3)_3$: yEu^{3+}	$Ba_3Tb(BO_3)_3$: xSm^{3+}	$Ba_3Tb(BO_3)_3$: yEu^{3+}